

Single and Double Nitroxide Labeled Bis(terpyridine)copper(II): The Influence of Multispin and Jahn-Teller Effects on PELDOR and RIDME[†]

Andreas Meyer^a, Dinar Abdullin^a, Gregor Schnakenburg^b, Olav Schiemann^{a,*}

^aRheinische Friedrich-Wilhelms-University Bonn, Institute of Physical and Theoretical
Chemistry, Wegelerstr. 12, 53115 Bonn, Germany. E-mail: schiemann@pc.uni-
bonn.de; Tel: +49 0228 732989

^bInstitute of Inorganic Chemistry, Rheinische Friedrich-Wilhelms-University Bonn,
Gerhard-Domagk-Str. 1, 53121 Bonn, Germany.

Supporting Information

| | |
|--|----|
| 1 Crystal structure of 2b and comparison with geometric parameters obtained from PeldorFit | 3 |
| 2 Pulse sequences used in this work | 10 |
| 3 EPR parameters and further EPR measurements on 2x and 2b. | 10 |
| 3.1 EPR spectra and EPR Parameters of 2x and 2b..... | 10 |
| 3.2 PELDOR and RIDME measurements on 2x and 2b..... | 12 |
| 3.3 Inversion recovery of the copper signal of 2x and 2b | 15 |
| 3.4 Phase memory times of the nitroxide and the copper signal in 2x and 2b | 17 |
| 4 Multispin effects in PELDOR of 2x and 2b | 19 |
| References | 24 |

1 Crystal structure of **2b** and comparison with geometric parameters obtained from PeldorFit

Clear green blocks of **2b**·4acetone·cyclohexane were obtained from a layered acetone/cyclohexane mixture. The data collection was performed on a STOE-IPDS-2T diffractometer (area detector) using graphite monochromated Mo- K_{α} radiation ($\lambda = 0.71073$ Å). The diffractometer was equipped with a low-temperature device (Cryostream 700er series, Oxford Cryosystems, 123 K). Intensities were measured by fine-slicing φ and ω -scans and corrected for background, polarization and Lorentz effects. A numerical absorption correction was applied for the data set. The structure was solved by direct methods and refined anisotropically by the least-squares procedure implemented in the ShelX program system.¹ Hydrogen atoms were included isotropically using the riding model on the bound carbon atoms.

CCDC-1441273 contains the supplementary crystallographic data for this paper, which can be obtained free of charge from The Cambridge Crystallographic Data Centre via www.ccdc.cam.ac.uk/data_request/cif.

Details of the X-ray diffraction experiment on **2b** are given in Table S1.

Table S1. Crystal data and structure refinement for the different X-ray experiments on compound **2b**.

| | |
|-------------------------------------|--|
| Empirical formula | C ₂₁₅ H ₂₁₈ Cu ₂ F ₂₄ N ₁₆ O ₂₁ P ₄ |
| Moiety formula | 2(C ₈₈ H ₇₀ CuN ₈ O ₆), 4(F ₆ P), 9(C ₃ H ₆ O), 2(C ₆ H ₁₂) |
| Formula weight | 4069.00 g/mol |
| Temperature | 123(2) K |
| Wavelength | 0.71073 Å |
| Crystal system, space group | triclinic, P -1 |
| Unit cell dimensions | a = 20.1608(8) Å $\alpha = 71.678(3)^\circ$ b = 22.3481(8) Å $\beta = 67.478(3)^\circ$ c = 25.7380(6) Å $\gamma = 86.691(3)^\circ$ |
| Volume | 10142.9(7) Å ³ |
| Z, Calculated density | 2, 1.332 g/cm ³ |
| Absorption coefficient | 0.332 mm ⁻¹ |
| F(000) | 4244.0 |
| Crystal size | 0.31 x 0.15 x 0.12 mm ³ |
| θ -range for data collection | 2.6 – 25.25° |

¹ G. M. Sheldrick, *Acta Cryst.*, **2008**, A64, 112-122.

| | |
|--|--|
| Limiting indices | $-20 \leq h \leq 24, -26 \leq k \leq 26, -24 \leq l \leq 30$ |
| Reflections collected / unique | 62874 / 36067 [$R_{\text{int}} = 0.0839$] |
| Completeness to $\theta = 25.25^\circ$ | 98.3 % |
| Absorption correction | Numerical |
| Max. and min. transmission | 0.9395 and 0.6176 |
| Refinement method | Full-matrix least squares on F^2 |
| Data / restraints / parameters | 36067 / 96 / 2573 |
| Goodness-of-fit on F^2 | 0.717 |
| Final R indices [$I > 2\sigma(I)$] | $R_1 = 0.0614, wR_2 = 0.1036$ |
| R indices (all data) | $R_1 = 0.1895, wR_2 = 0.1242$ |
| Largest diff. peak / hole | 0.570 and $-0.340 \text{ e}\text{\AA}^{-3}$ |

2b crystallizes in the triclinic space group $P\bar{1}$. The asymmetric unit (Figure S1) contains two independent cations **A** and **B** which differ slightly in their geometric parameters. Relevant geometrical parameters for the two different cations of **2b** as obtained from the crystal structure are defined in Figure S2 and listed in Table S2. In addition to the parameters defined in Figure S2, the angles ψ and χ between the mean planes of the pyrrolidine-*N*-oxides and the g_x, g_z plane of the copper center are given in Table S2 (see also Figure S3).

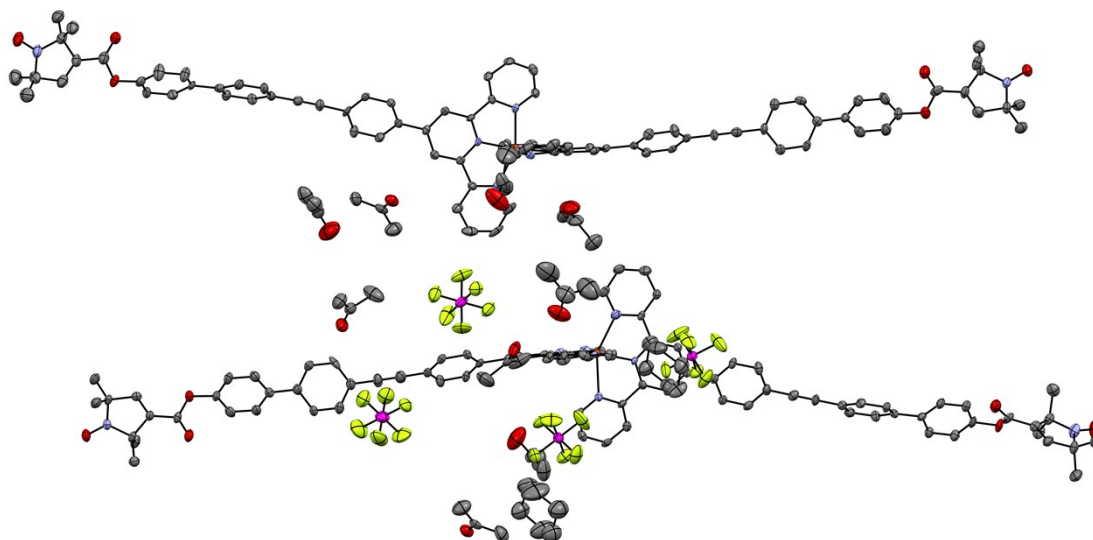


Figure S1. The asymmetric unit of the unit cell of **2b**. Red atoms = O, blue atoms = N, grey atoms = C, dark orange atom = Cu, yellow atoms = F, purple atoms = P. Hydrogen atoms have been omitted for clarity.

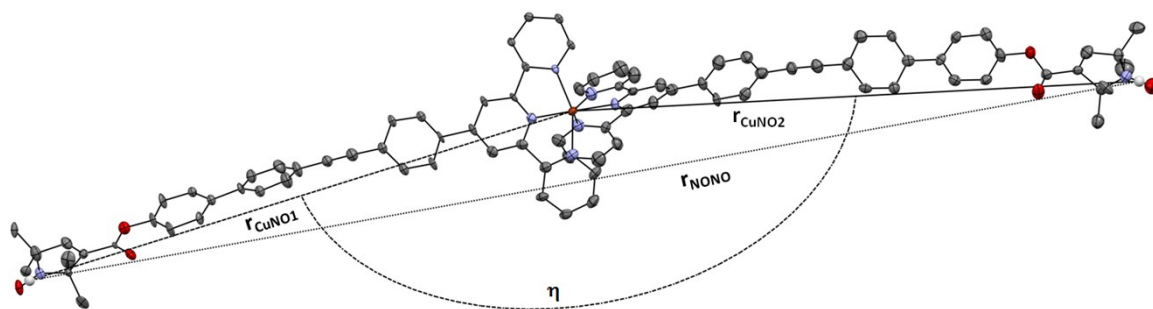


Figure S2. One exemplary complex cation from the crystal structure of **2b** to illustrate the meaning the distance parameters and the angle η as discussed in the text. Red atoms = O, blue atoms = N, grey atoms = C, dark orange atom = Cu. Hydrogen atoms have been omitted for clarity.

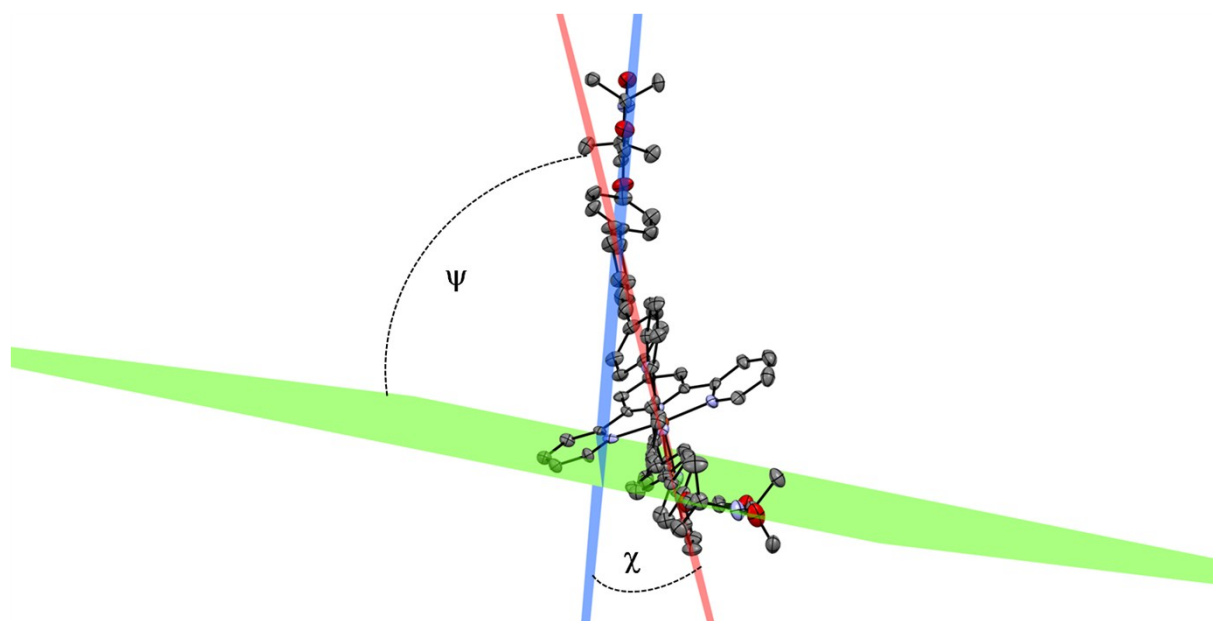


Figure S3. One exemplary complex cation from the crystal structure of **2b** to illustrate the meaning of the angles ψ and χ as discussed in the text. Red atoms = O, blue atoms = N, grey atoms = C, dark orange atom = Cu. Hydrogen atoms have been omitted for clarity.

Table S2. Geometrical parameters for the independent complex cations in the crystal structure of **2b**.

| | r_{CuNO1} [Å] | r_{CuNO2} [Å] | $\langle r_{\text{CuNO}} \rangle$ [Å] | r_{NONO} [Å] | η [deg] | ψ [deg] | χ [deg] |
|----------|------------------------|------------------------|---------------------------------------|-----------------------|--------------|--------------|--------------|
| A | 26.42 | 26.44 | 26.43 | 51.98 | 156.8 | 19.2 | 66.8 |
| B | 26.46 | 26.62 | 26.54 | 52.00 | 159.0 | 70.1 | 78.5 |

All geometrical parameters given in Table S2 are taken from the crystal structure and are related to the geometric parameters optimized by PeldorFit. The original geometric parameters from PeldorFit (the mean values of the inter-spin distance and the five angles describing the positions and relative orientations of the spin centers and the corresponding distribution widths) were varied in the ranges specified in our previous publication.¹ The distances are the main parameter of interest in the PELDOR experiments and detailed analysis of the independent cations in the crystal structure allows giving estimates about the range of distances to expect. The angle α is the angle between the two vectors interconnecting one nitroxide with the copper

spin center. Note, that these vectors are similarly aligned as the N-O bond (and thereby the g_x component) of the nitroxides and the bonds of the copper atom to the nitrogen donors of the central pyridine rings of the tpy ligands (and thereby the g_z component of the copper spin center). The relation between the geometric structure and the orientation of the g tensor of the copper terpyridine center is also discussed in the main text and in a previous study in greater detail.² The g tensor coordinate system for a copper terpyridine complex elongated along the molecular x axis is shown in detail in Figure S4. The orientation of the g tensor in Figure S4 was obtained using DFT calculations (B3LYP functional with TZVPP basis sets as implemented in ORCA³). The structure of cation **F** from the crystal structure¹ of the unsubstituted (bis(terpyridine))copper(II) bis(tetraphenylborate) was used as input geometry. The obtained orientation of the g tensor with respect to the molecular geometry agrees completely with those given in the aforementioned study.

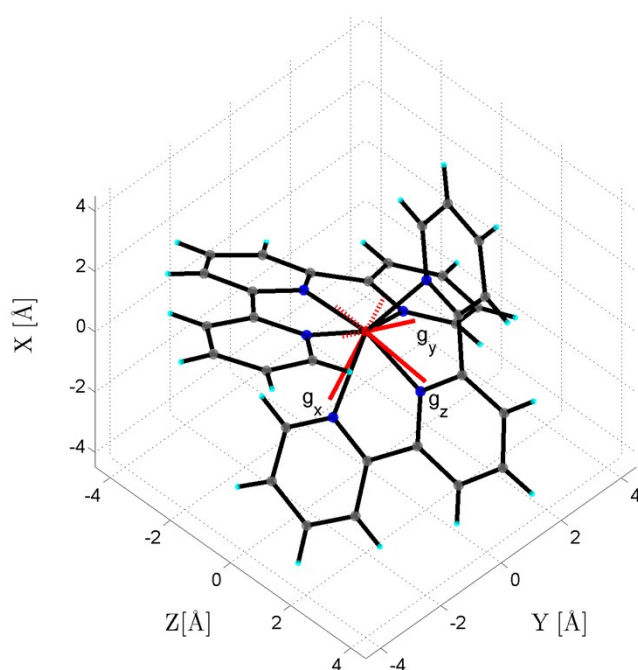


Figure S4. g tensor frame-work of the terpyridine ligated copper center. Red atom = Cu; Blue atoms = N; Grey atoms = C, Teal atoms = H.

Importantly, the vectors, which interconnect the nitroxides and the copper center are parallel to the parallel component of the dipolar coupling tensor. This is of importance for the EPR based distance measurements, as it implies that selectivity for the g_z value of the copper center is also selective for the parallel component of the dipolar coupling tensor, although the bent structure of the complex **2b** leads to deviations from perfect colinearity. The effects of the bending of the molecule can be estimated by inspecting the structure of the two independent cations in the crystal structure of

2b. A noteworthy feature about the molecular bending is that it appears to occur around the g_y axis of the copper center and is brought about by non-symmetric displacements of the remote pyridine rings as illustrated in Figure S5. The complexes in the crystal structure of **2b** have that in common with the most strongly distorted cation **F** of the unsubstituted (bis(terpyridine))copper(II) bis(tetraphenylborate) which is shown in Figure S4.

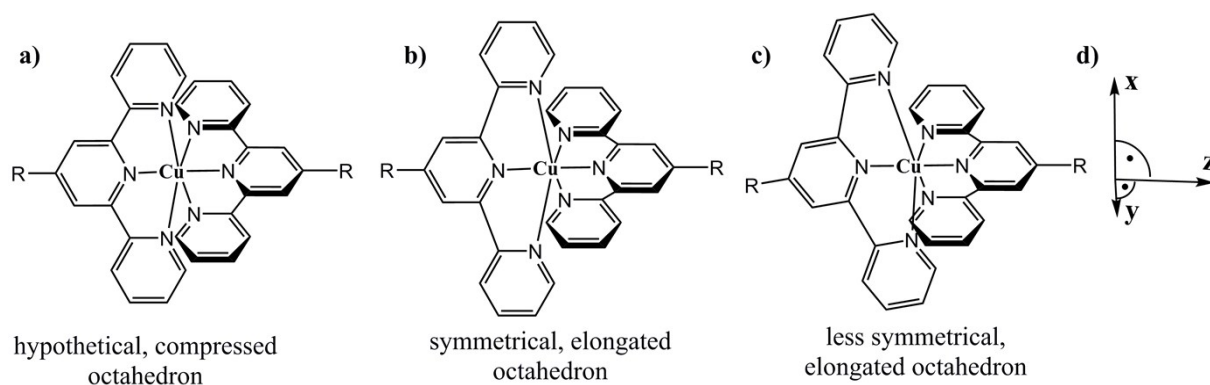


Figure S5. Schematic coordination geometries of the cations of **2b** (a – c) and approximate g tensor coordinate system (d).

Taking together the features discussed above and illustrated in Figures S2 - S5 reveals that η is related to the angle ζ in the program PeldorFit, which defines the angle between the interspin vectors and the highest g value of the observer spin (i.e. the copper centered spin).¹ Therefore, ζ should be approximately equal to $\eta/2$, which is indeed found by PeldorFit. Similarly, the angle ϕ defined as the angle between the interspin vector and the smallest g value of the copper center can be estimated to be close to $90 - \alpha/2$. This is indeed found using PeldorFit as shown in Table S3.

Table S3. Geometric parameters obtained from PeldorFit and from the crystal structure of **2b**.

| | r [nm] | ζ [°] | ϕ [°] |
|---------------------------------|-------------|-------------|-------------|
| 2x | 2.58 | 81.4 | 5.5 |
| 2b | 2.60 | 82.1 | 0.7 |
| 2b (acidic) | 2.57 | 76.4 | 37.2 |
| 2b (crystal)^a | 2.64 – 2.66 | 78.4 – 79.5 | 10.5 – 11.6 |

^a All parameter values are taken from Table S1. Instead of giving average values and standard deviations, the highest and lowest values for each parameter have been given in order to specify a range of expected values. The values for ζ and ϕ are calculated for the crystal structure as described in the text.

The values listed in table S3 are those which are in our experience more reliable than the Euler angles, as defined in PeldorFit.¹ The Euler angles α , β and γ on the other hand usually do not show clearly defined minima. The reason for that is the low resolution of the g tensor of the nitroxide and the two lower g values of the copper g tensor at X-band frequency. Therefore, the PeldorFit data do not allow analyzing the angles ψ and χ in frozen solution EPR samples. To further quantify the analysis of the PeldorFit parameters, error profiles of each PeldorFit parameter were calculated. In these calculations, one parameter and its width were varied while all other parameters were kept at their optimum values. The results of these calculations are shown in Figures S6 - S8.

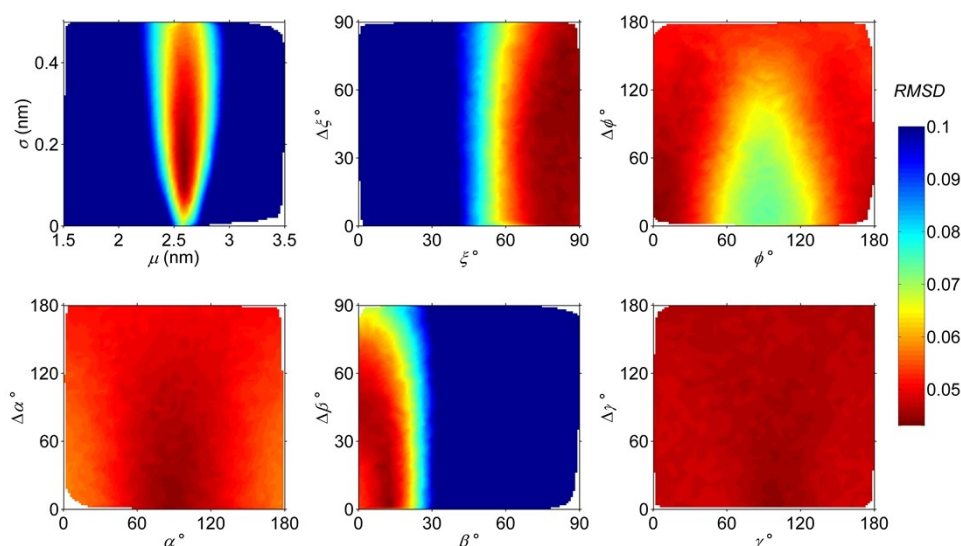


Figure S6. Error profiles for each PeldorFit parameter for measurements of **2x** in neutral solution (DMSO/MeOH, 1:1.5)

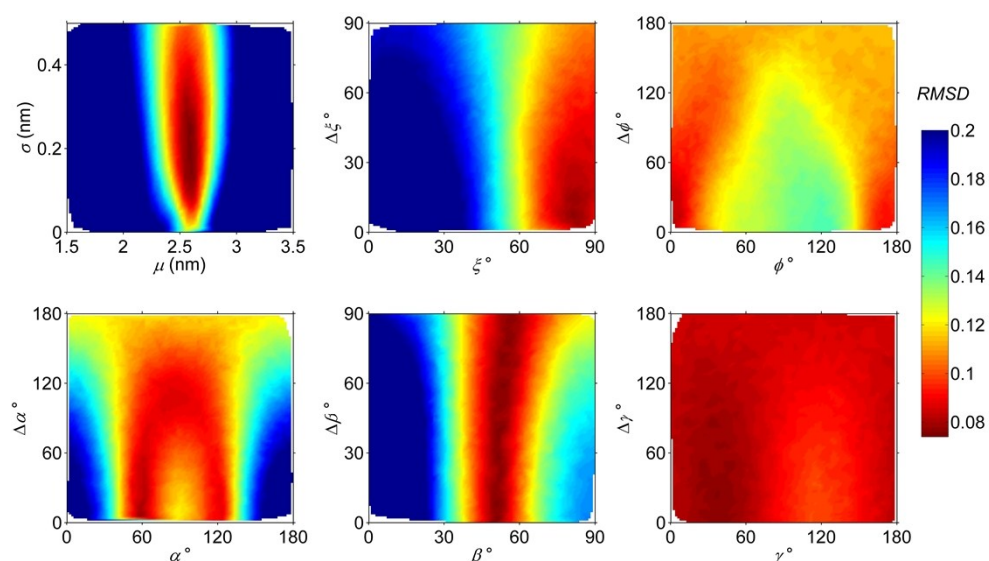


Figure S7. Error profiles for each PeldorFit parameter for measurements of **2b** in neutral solution (DMSO/MeOH, 1:1.5)

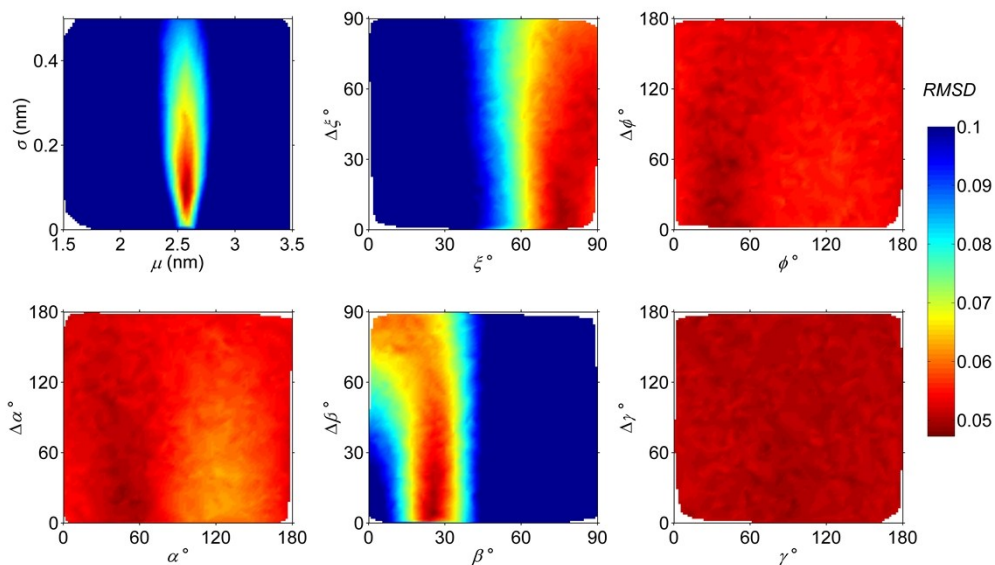
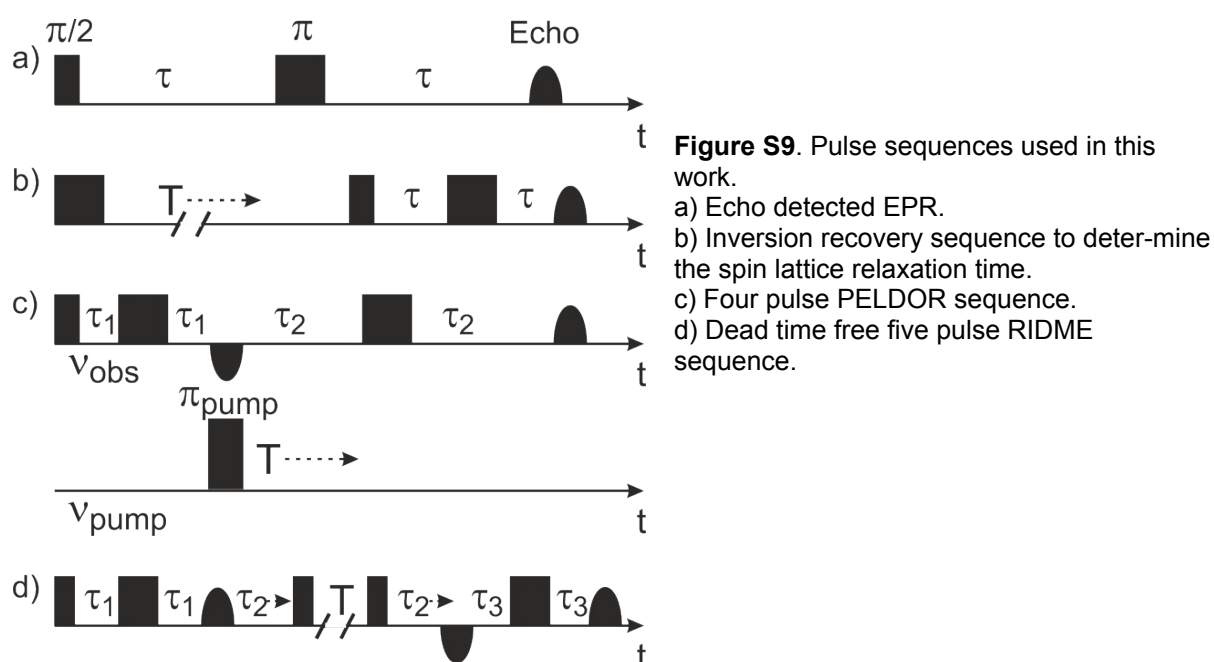


Figure S8. Error profiles for each PeldorFit parameter for measurements of **2b** in acidic solution (DMSO/MeOH, 1:1.5)

For all samples (**2x**, **2b**, and **2b** under acidic conditions) an optimum distance is found to be located in a narrow minimum along the distance axis. The width of the distance distribution σ on the other hand is not very strongly defined for **2a** and **2b** in neutral solutions. In acidic solution, this value is has a narrower minimum in the error profile. The error profiles for ζ look similar for all samples. This is expected, as the geometries observed crystallographically and those discussed in the main text for the acidic sample of **2b** each have similar orientations of the g tensor of the copper centered spin and the copper-nitroxide vector. The angle ϕ , which relates the lowest g tensor value of the observer spin and the interspin vector, is less well defined for all samples. Especially, under acidic conditions it is nearly undefined. Since the lowest and the intermediate g tensor value of the copper g tensor are similar under neutral and nearly equal under acidic conditions this seems reasonable. At least one of the Euler angles in each sample is completely undefined. As these angles are strongly interrelated, none of the Euler angles should be considered as clearly defined, even if a clear minimum occurs in the error profiles. As shown in the original publication, several symmetry related, equivalent solutions are obtained with respect to the angular parameters used by PeldorFit.

2 Pulse sequences used in this work

Figure S9 summarizes the pulse sequences used in this work



3 EPR parameters and further EPR measurements on 2x and 2b.

In the following subsections, the measurement parameters and parameters used to simulate the obtained data are detailed. Furthermore, data which was not shown in the main text is presented. Most experiments have been conducted in neutral and acidic solution. While the parameters used for the simulation of the data differs for the two types of solution, the measurement parameters are identical for both types of solution, unless otherwise specified.

3.1 EPR spectra and EPR Parameters of 2x and 2b

EPR spectra of **2x** and **2b** have been obtained using a two pulse echo sequences and are shown in the main text. The g values and hyperfine coupling constants A of **2x** and **2b** have been obtained by simulating these spectra. The simulation parameters are listed in Table S4 for neutral solutions and in Table S5 for acidic solutions. The measurement parameters used to obtain the echo detected EPR spectra for both kinds of solution are listed in Table S6.

Table S4. Parameters used to simulate the EPR spectra of **2x** and **2b** in neutral solution at X- and Q-band.

| Compound | 2x | 2b | 2x | 2b |
|------------------|--------|--------|--------|--------|
| MW-Band | X | X | Q | Q |
| g_x (Cu) | 2.256 | 2.256 | 2.257 | 2.256 |
| g_y (Cu) | 2.093 | 2.093 | 2.092 | 2.093 |
| g_z (Cu) | 2.042 | 2.042 | 2.043 | 2.042 |
| A_x (Cu) [MHz] | 455 | 455 | 455 | 455 |
| A_y (Cu) [MHz] | 70 | 70 | 70 | 70 |
| A_z (Cu) [MHz] | -90 | -90 | -90 | -90 |
| g_x (NO) | 2.0085 | 2.0085 | 2.0091 | 2.0091 |
| g_y (NO) | 2.0063 | 2.0063 | 2.0075 | 2.0075 |
| g_z (NO) | 2.0025 | 2.0025 | 2.0024 | 2.0024 |
| A_x (NO) [MHz] | 11 | 11 | 15 | 15 |
| A_y (NO) [MHz] | 16 | 16 | 15 | 15 |
| A_z (NO) [MHz] | 95 | 95 | 95 | 95 |

Table S5. Parameters used to simulate the EPR spectra of **2x** and **2b** in acidic solution at X- and Q-band.

| Compound | 2x | 2b | 2x | 2b |
|------------------|--------|--------|--------|--------|
| MW-Band | X | X | Q | Q |
| g_x (Cu) | 2.268 | 2.268 | 2.265 | 2.265 |
| g_y (Cu) | 2.063 | 2.064 | 2.062 | 2.062 |
| g_z (Cu) | 2.060 | 2.064 | 2.058 | 2.060 |
| A_x (Cu) [MHz] | 505 | 502 | 510 | 507 |
| A_y (Cu) [MHz] | -55 | -55 | -50 | -50 |
| A_z (Cu) [MHz] | -65 | -65 | -65 | -65 |
| g_x (NO) | 2.0088 | 2.0088 | 2.0091 | 2.0091 |
| g_y (NO) | 2.0065 | 2.0065 | 2.0075 | 2.0075 |
| g_z (NO) | 2.0025 | 2.0025 | 2.0024 | 2.0024 |
| A_x (NO) [MHz] | 11 | 11 | 15 | 15 |
| A_y (NO) [MHz] | 16 | 16 | 15 | 15 |
| A_z (NO) [MHz] | 95 | 95 | 95 | 95 |

Table S6. Measurement parameters used to obtain echo detected EPR spectra of **2x** and **2b** at X- and Q-band.

| Compound | 2x | 2b | 2x | 2b |
|-----------------------|-----|-----|-----|-----|
| MW-Band | X | X | Q | Q |
| p_1 [ns] | 12 | 10 | 20 | 22 |
| p_2 [ns] | 24 | 20 | 20 | 22 |
| τ [ns] | 140 | 140 | 440 | 440 |
| SRT [μ s] | 997 | 997 | 997 | 997 |

p_1 = length of first pulse, p_2 = length of second pulse, t = separation between first and second pulse, SRT = shot repetition time.

The acquisition gate was set to cover the whole optimized echo and about 20 ns of at each side of the optimized echo. The shot repetition times are adjusted to allow for

fast acquisition of the copper signal. If the nitroxide signal is to be observed (as in RIDME), longer short repetition times are necessary.

3.2 PELDOR and RIDME measurements on 2x and 2b

The parameters of the PELDOR measurements on **2x** and **2b** at X-band frequencies are given in Table S7. Identical parameters have been used for **2x** and **2b**. The copper signal was used for observation and the detection frequency was set to about 150 MHz to the high frequency side of the resonator dip.

Table S7. Parameters of the PELDOR measurements on **2x** and **2b** at X-band frequencies.

| $\Delta\nu$ [MHz] | 150 | 300 | 450 | 600 |
|-----------------------|------------|------------|------------|------------|
| p_1 [ns] | 12 | 12 | 12 | 12 |
| p_2 [ns] | 24 | 24 | 24 | 24 |
| P_{pump} [ns] | 18 | 26 | 26 | 56 |
| τ [ns] | 140 | 140 | 440 | 440 |
| SRT [μ s] | 9900 | 9900 | 9900 | 9900 |
| B_0 [mT] | 345.2 | 340.2 | 334.8 | 329.5 |

The nitroxide-nitroxide distance determination was performed at Q-band frequencies as at X-band frequencies the nitroxide and copper signal overlap. The parameters are listed in Table S8. The parameters obtained using PeldorFit are discussed in the main text and listed in the section concerned with the crystal structure of **2b**.

Table S8. Parameters of the internitroxide PELDOR measurements on **2x** and **2b** at Q-band frequencies.

| Species | 2x | 2b |
|-----------------------|-----------|-----------|
| ν_{obs} [GHz] | 33.777 | 33.941 |
| $\Delta\nu$ [MHz] | 70 | 70 |
| p_1 [ns] | 14 | 12 |
| p_2 [ns] | 28 | 24 |
| P_{pump} [ns] | 24 | 26 |
| τ [ns] | 460 | 460 |
| SRT [μ s] | 9900 | 9900 |
| B_0 [mT] | 1203.9 | 1209.4 |

The RIDME experiment in neutral solution was conducted at X- and Q-Band frequencies. Identical parameters have been used for **2x** and **2b**. The parameters are listed in Table S9. The individual RIDME time traces at X- and Q-band frequencies are shown in Figures S10 and S11.

Table S9. Parameters of the RIDME measurements on **2x** and **2b** at both MW bands.

| MW-band | X | Q |
|------------------|------|------|
| $P_{\pi/2}$ [ns] | 10 | 14 |
| P_{π} [ns] | 20 | 28 |
| τ_1 [ns] | 140 | 440 |
| τ_2 [ns] | 180 | 420 |
| T [μ s] | 100 | 80 |
| SRT [μ s] | 9900 | 9900 |

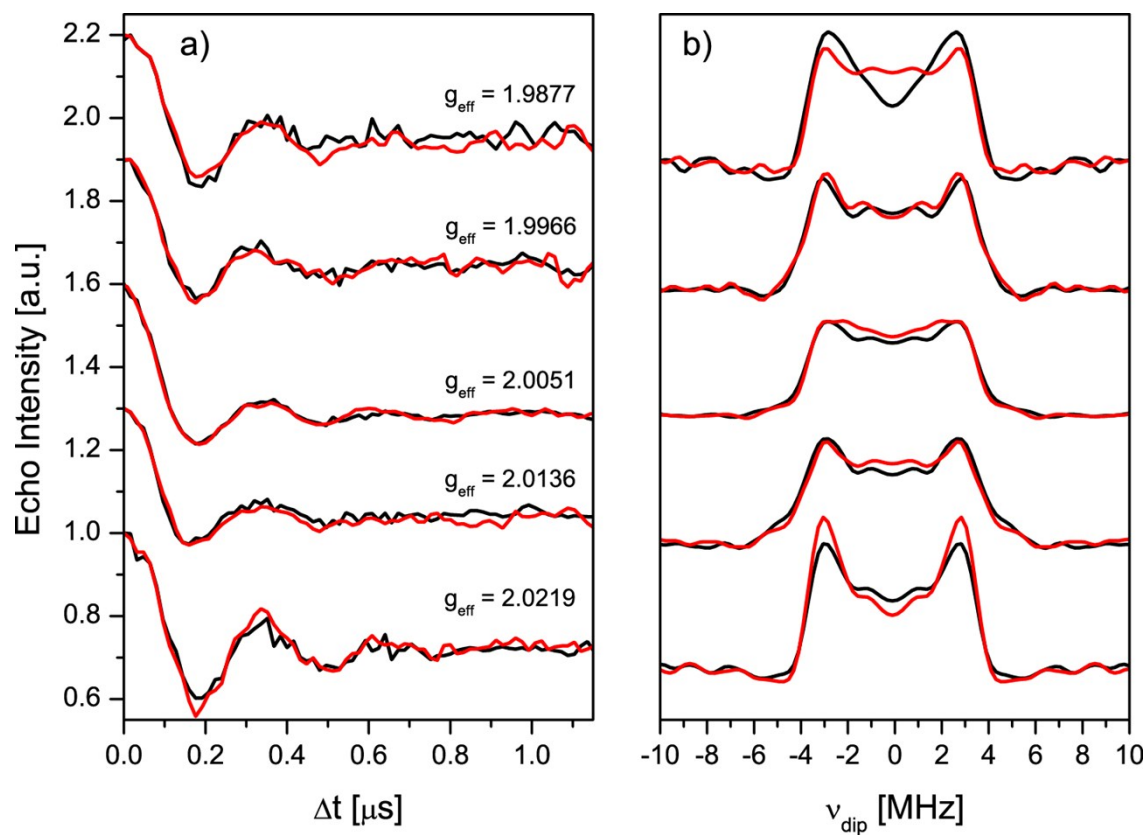


Figure S10. RIDME time traces and their Fourier transforms (a) and b), respectively) at different effective g values of the nitroxide signal position recorded at X-band frequencies of **2x** (black lines) and **2b** (red lines).

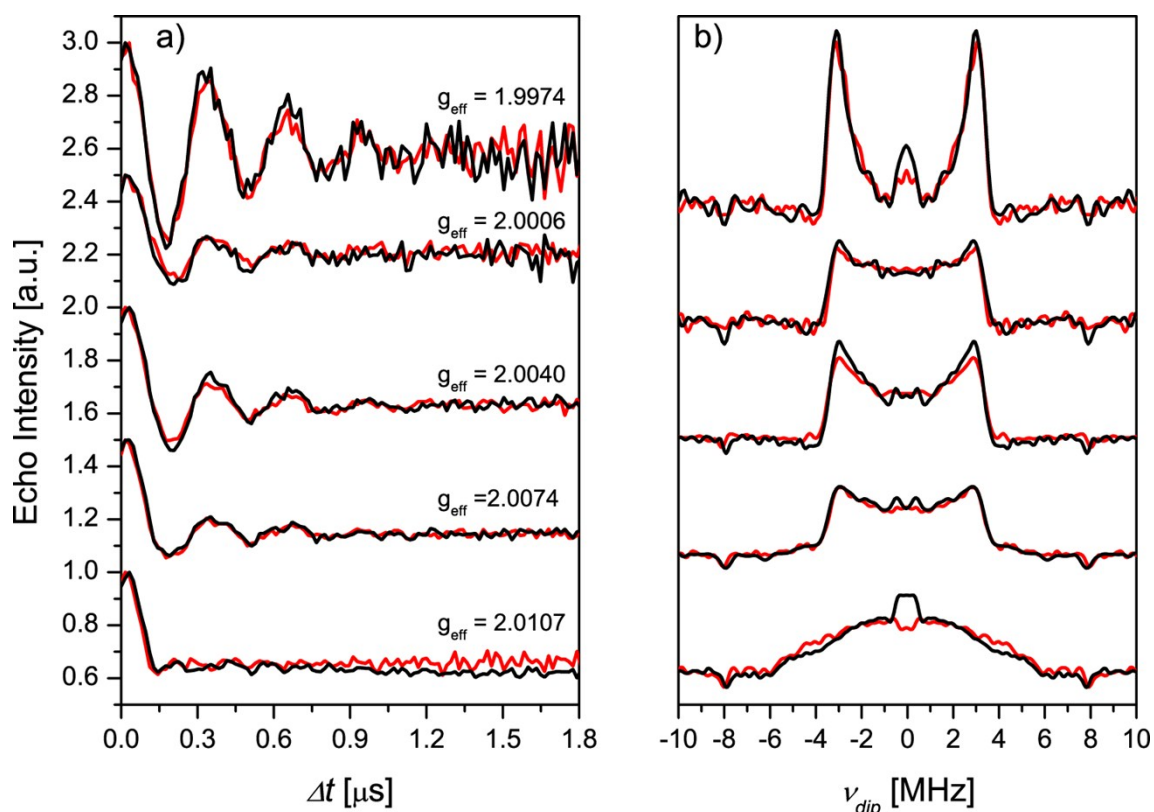


Figure S11. RIDME time traces and their Fourier transforms at different effective g values of the nitroxide signal position recorded at Q-band frequencies of **2x** (black lines) and **2b** (red lines).

The RIDME experiment was also conducted in acidic solution for **2b** at Q-band frequencies (Figure S12).

For the measurements in acidic solution, the interpulse separation has been increased by a factor of 4.5 with respect to the measurement in neutral solution, in accordance with the results obtained using the inversion recovery experiment. The obtained modulation depths are now approximately 50% lower than in neutral methanolic solutions. This is expected, if one of the nitroxide ligands is completely removed from complex **2b** as discussed in the main text. With respect to orientation selection, similar results as in neutral solution are obtained, as the orientations election is entirely determined by the selection of the nitroxide part of the EPR signal and the nitroxide signal is not affected by addition of acid to the solvent system. Besides having a lower modulation depth, the overall quality of the obtained data is worse than for neutral solution. For example, a larger residual contribution of the deuteron modulation is visible in the RIDME time traces. This observation is attributed to the fact, that the echo signal used to record the RIDME time trace is comprised of two contributions in equal weight, namely the nitroxides still bound to the copper center and the nitroxides which are removed from the copper center and

therefore do not show modulations owed to electron electron coupling. As the obtained time trace is a sum of two contributions, removal of the ESEEM modulations as described for the time traces in neutral solution might be less efficient. Despite the reduced data quality, a mean copper-nitroxide distance of 2.48 ± 0.06 nm could be obtained, which is slightly lower than the value observed in neutral solution.

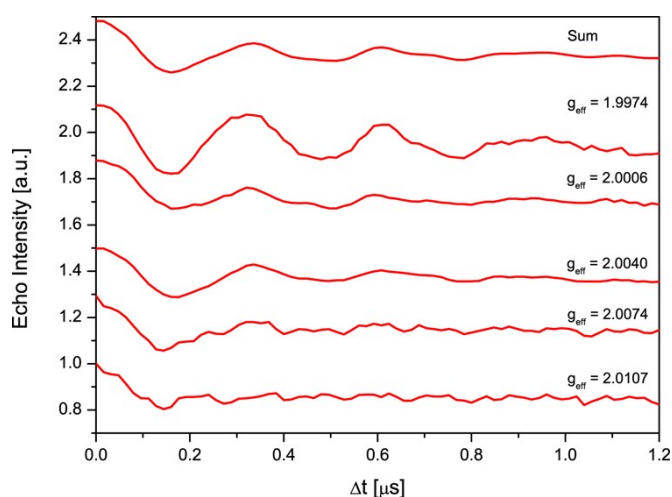


Figure S12. RIDME time traces of **2b** in acidic solution and their Fourier transforms at different effective g values of the nitroxide signal position recorded at Q-band frequencies.

As mentioned in the main text, the nitroxide nitroxide distance could no longer be measured in **2b** in the acidified solvent system. The corresponding time trace is shown in Figure S13.

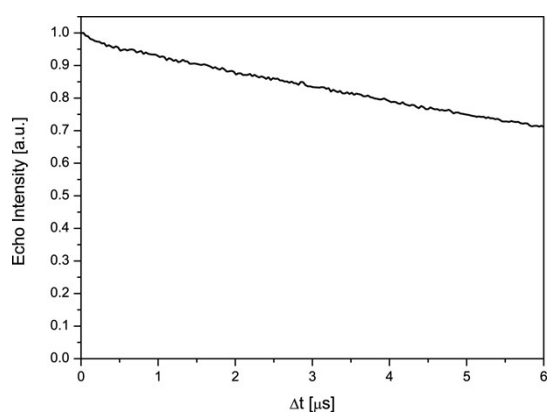


Figure S13. PELDOR measurement of the nitroxide nitroxide distance in **2b** in the acidified solvent system (deuterated DMSO/MeOD, 1:1.5, acidified using H_2SO_4) at Q-band frequency.

3.3 Inversion recovery of the copper signal of 2x and 2b

The spin lattice relaxation times of the copper signal of **2x** and **2b** have been measured using the inversion recovery sequence. The inversion recovery time traces

have been fitted empirically using equation (S1) for the echo intensity I as a function of the interpulse separation T .

$$I = I_0 \left(1 - ae^{-T/T_1^a} - be^{-T/T_1^b} \right) \text{ with } a + b = 1 \quad (\text{S1})$$

The results of the inversion recovery experiments for neutral solutions are summarized in Figure S14 and Table S11.

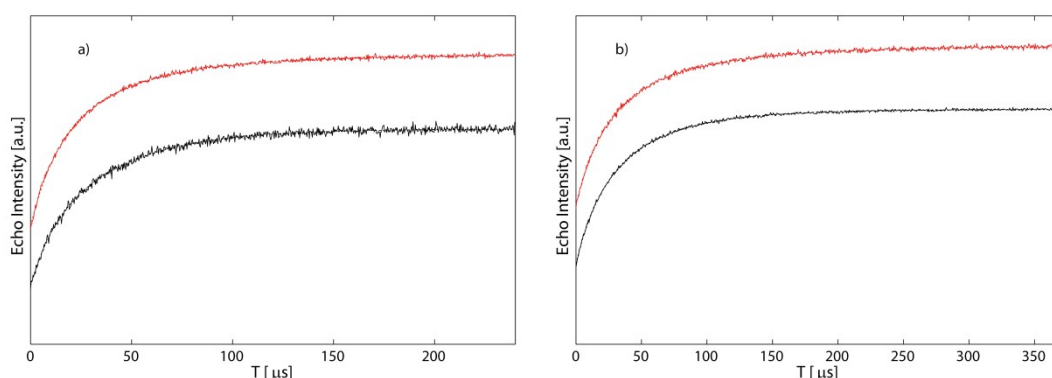


Figure S14. Inversion recovery time traces of **2x** (black lines) and **2b** (red lines) and corresponding biexponential fitting functions (dashed lines) at a) X-band frequencies in DMSO/MeOH (1:1.5) and b) Q-band frequencies in d_6 -DMSO/MeOD (1:1.5). The inversion recovery time traces have been recorded at the maximum intensity of the copper signal. Fitting and measurement parameters are given in Tables S10 and S11.

Table S10. Fitting Parameters of the inversion recovery time traces

| Compound and MW frequency | a | T_1^a [μs] | b | T_1^b [μs] | T_1^{av} [μs] |
|---------------------------|-----------------|---------------------------|-----------------|---------------------------|------------------------------|
| 2x , X | 0.74 ± 0.03 | 38.8 ± 0.9 | 0.26 ± 0.03 | 9.8 ± 0.9 | 31.3 |
| 2b , X | 0.53 ± 0.01 | 44.6 ± 0.9 | 0.47 ± 0.01 | 12.8 ± 0.9 | 29.7 |
| 2x , Q | 0.59 ± 0.02 | 51.9 ± 0.8 | 0.41 ± 0.02 | 17.0 ± 0.5 | 37.6 |
| 2b , Q | 0.47 ± 0.02 | 72.0 ± 2.0 | 0.53 ± 0.02 | 19.8 ± 0.6 | 44.3 |

Table S11. Measurement parameters used to obtain echo detected EPR spectra of **2x** and **2b** at X- and Q-band.

| Compound | 2x | 2b | 2x | 2b |
|------------------------------|-----------|-----------|-----------|-----------|
| MW-Band | X | X | Q | Q |
| p_1 [ns] | 24 | 20 | 28 | 28 |
| p_2 [ns] | 12 | 10 | 14 | 14 |
| p_3 [ns] | 24 | 20 | 28 | 28 |
| T [ns] | 1000 | 1000 | 1000 | 1000 |
| τ [ns] | 200 | 200 | 440 | 440 |
| SRT [μs] | 1910 | 1910 | 997 | 997 |

p_1 = length of first pulse, p_2 = length of second pulse, p_3 = length of third pulse, T = separation between first and second pulse, τ = separation between second and third pulse, SRT = shot repetition time.

The inversion recovery was repeated for **2x** and **2b** in acidic solution at X-band frequency and for **2b** also at Q-band frequency. The results are summarized in Figure S15 and Table S12. Noteworthy, the spin lattice relaxation time of the copper spin center differed very strongly from the spin lattice relaxation time in neutral solution (Figure S15 and Table S12).

The strong increase of the spin lattice relaxation by one order of magnitude is another hint for the presence of different species (i.e. copper complexes in which one terpyridine based ligand has been replaced by solvent molecules), as identical species with just slight differences in the details of the first coordination sphere would probably have very similar relaxation behavior.

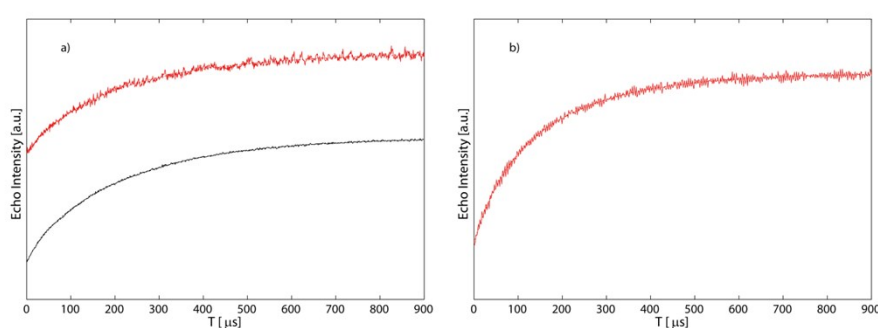


Figure S15. Inversion recovery time traces of spectra of **2x** (black lines) and **2b** (red lines) and their simulations (dashed lines) in 0.1 M sulfuric acid solutions at a) X-band frequencies (MeOH and DMSO, 1.5:1) and b) Q-band frequencies (MeOD and d_6 -DMSO, 1.5:1). The inversion recovery time traces have been recorded at the maximum intensity of the copper signal. Fitting parameters are given in Tables S12.

Table S12. Fitting parameters of the inversion recovery time traces in acidic solutions.

| Compound and MW frequency | a | T_1^a [μ s] | b | T_1^b [μ s] | T_1^{av} [μ s] |
|---------------------------|-----------------|--------------------|-----------------|--------------------|-----------------------|
| 2x , X | 0.88 ± 0.01 | 231.0 ± 1.0 | 0.12 ± 0.01 | 38.0 ± 2.0 | 207.8 |
| 2b , X | 0.70 ± 0.04 | 280.0 ± 10.0 | 0.30 ± 0.04 | 90.0 ± 10.0 | 223.0 |
| 2b , Q | 0.72 ± 0.03 | 196.0 ± 5.0 | 0.28 ± 0.02 | 57.0 ± 5.0 | 157.1 |

3.4 Phase memory times of the nitroxide and the copper signal in **2x** and **2b**

The phase memory times of the observed spin coherences strongly affect the sensitivity of both the PELDOR and the RIDME experiments. The copper signal was not used for observation at Q-band frequencies and was therefore not measured. The phase memory times T_M of **2x** and **2b** have been measured using the two pulse ESEEM sequence. The results of these measurements are shown in Figures S16 - S18.

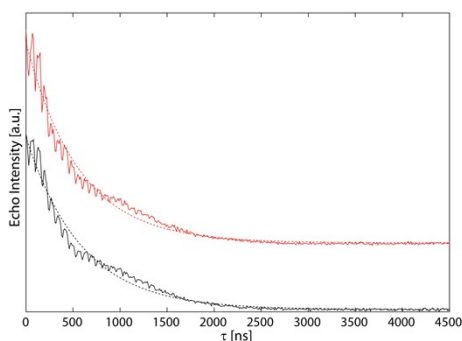


Figure S16. Two pulse ESEEM time traces (full lines) and simulations of the background function (dashed lines) of the copper signal of **2x** (black lines) and **2b** (red lines) in DMSO/MeOH (1:1.5) at X-band MW frequencies and a temperature of 20 K. The ESEEM time traces have been recorded at the maximum intensity of the copper signal.

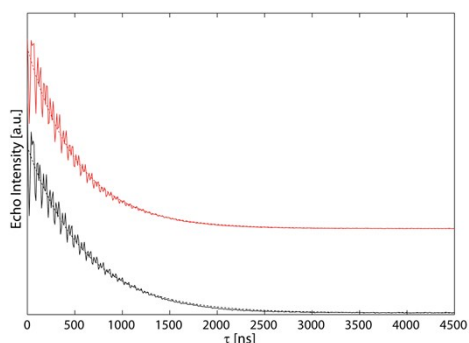


Figure S17. Two pulse ESEEM time traces (full lines) and the simulations of the background function (dashed lines) of the nitroxide signal of **2x** (black lines) and **2b** (red lines) in DMSO/MeOH (1:1.5) at X-band MW frequencies and a temperature of 20 K. The ESEEM time traces have been recorded at the maximum intensity of the nitroxide signal.

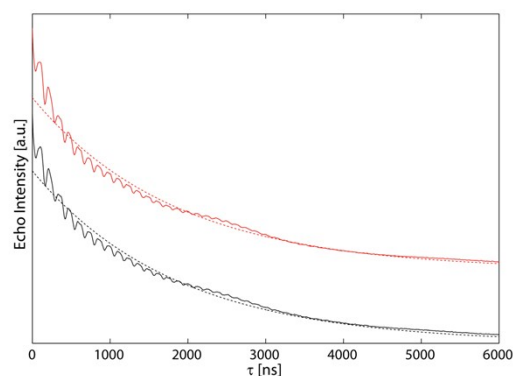


Figure S18. Two pulse ESEEM time traces (full lines) and simulations of the background function (dashed lines) of the nitroxide signal of **2x** (black lines) and **2b** (red lines) in d₆-DMSO/MeOD (1:1.5) at Q-band MW frequencies and a temperature of 20 K. The ESEEM time traces have been recorded at the maximum intensity of the copper signal.

The ESEEM time traces have been fitted empirically using equation (S2) for the echo intensity I as a function of the interpulse separation τ .

$$I = I_0 e^{-\tau/T_M} \quad (\text{S2})$$

The obtained Fitting parameters are given in Table S13.

Table S13. Fitting parameters of the two pulse ESEEM time traces of **2x** and **2b** at X- and Q-band (T = 20 K).

| Compound and MW frequency | $T_M^{Cu}(X)$ [ns] | $T_M^{NO}(X)$ [ns] | $T_M^{NO}(Q)$ [ns] |
|---------------------------|--------------------|--------------------|--------------------|
| 2x | 590 ± 5 | 605 ± 5 | 1835 ± 5 |
| 2b | 560 ± 5 | 530 ± 5 | 1934 ± 5 |

At X-band, a mixture of DMSO and MeOH was used as solvent system (1:1.5). The occurrence of very strong deuteron modulations prevented the use of deuterated solvents at X-band frequency, as a complete removal of the deuteron modulations in the RIDME experiment could not be achieved. At Q-band frequency, the deuteron modulations are not as strong as at X-band frequency and could be removed from the RIDME time traces. The strongly increased phase memory times at Q-band frequencies are probably primarily owed to the use of deuterated solvents (changes in that order of magnitude have been reported before).⁴ The measurement parameters are given in Table S14 and have been chosen identical for the copper and nitroxide signal, except for the *SRT*.

Table S14. Measurement parameters of the two pulse ESEEM time traces of **2x** and **2b** at X- and Q-band.

| MW-band | X | Q |
|------------------------------|----------|------|
| $P_{\pi/2}$ [ns] | 10 | 14 |
| P_{π} [ns] | 20 | 28 |
| <i>SRT</i> ^a [μs] | 300/9900 | 9900 |

^a *SRT*s for the copper and nitroxide signal, respectively.

4 Multispin effects in PELDOR of **2x** and **2b**

As mentioned in the main text, the occurrence of combination frequencies owed multispin effects can change the PELDOR form factor markedly. The occurrence of combination frequencies could manifest itself in the appearance of further extrema in the time traces, a shift of the existing extrema or a more pronounced damping to

name ea few possibilities. However, none of the aforementioned effects is observed. Aside from the increased modulation depth only subtle differences occur in the formfactor of the PELDOR time traces of **2x** and **2b**. As samples of **2x** always contain **2b** in relatively large fractions (~33%) the identification of multispin effects is further hampered. Three methods to investigate the origin of these slight deviations have been chosen: First, the PELDOR experiments on **2b** have been repeated using an ELDOR attenuation of 20 dB. The results of these measurements are shown and discussed in the main text and also in Figure S19. Secondly, the PELDOR measurements on **2b** have been repeated using the nitroxide for observation. As the copper is used for pumping and only one copper per molecule is available for pumping, no multispin effects are expected to occur using this set-up. The corresponding time traces are shown in Figure S19.

In accordance with the results obtained using the high ELDOR attenuation, no large changes of the formfactor are observed if the nitroxide is used for observation at any of the used frequency offsets. Surprisingly, the time trace at an offset of 150 MHz shows a large contribution owed to a low frequency modulation. The deviations caused by this low frequency modulation exceed those observed using any of the other measurement set-ups. As it was not possible to use the same pulse lengths using the “inverted” set-up as for the normal set-up (i.e. using copper for observation), an in depth analysis of the origin of this low frequency modulation is very difficult. An attempted analysis would be further complicated by the fact, that the nitroxide and copper signals overlap and therefore both contribute to the observed echo. Besides the pronounced low frequency modulation observed at 150 MHz frequency offset, no marked changes are observed using the inverted set-up. The absence of marked changes in both the attenuated and the inverted PELDOR experiment seem to corroborate the hypothesis, that multispin effects do not cause a marked change in the PELDOR formfactor. Finally, in addition to these experimental approaches, PELDOR time traces in which multispin effects are accounted for have been calculated. To do so the equations given by von Hagens *et al.*⁵ have been combined with the orientation selection calculated by PeldorFit. In addition to this, one needs to consider orientation correlation of all three spin centers. Although the crystal structure implies a slight bending between the two copper nitroxide vectors (angle $\alpha < 180^\circ$) a fully stretched complex geometry with $\alpha = 180^\circ$ has been

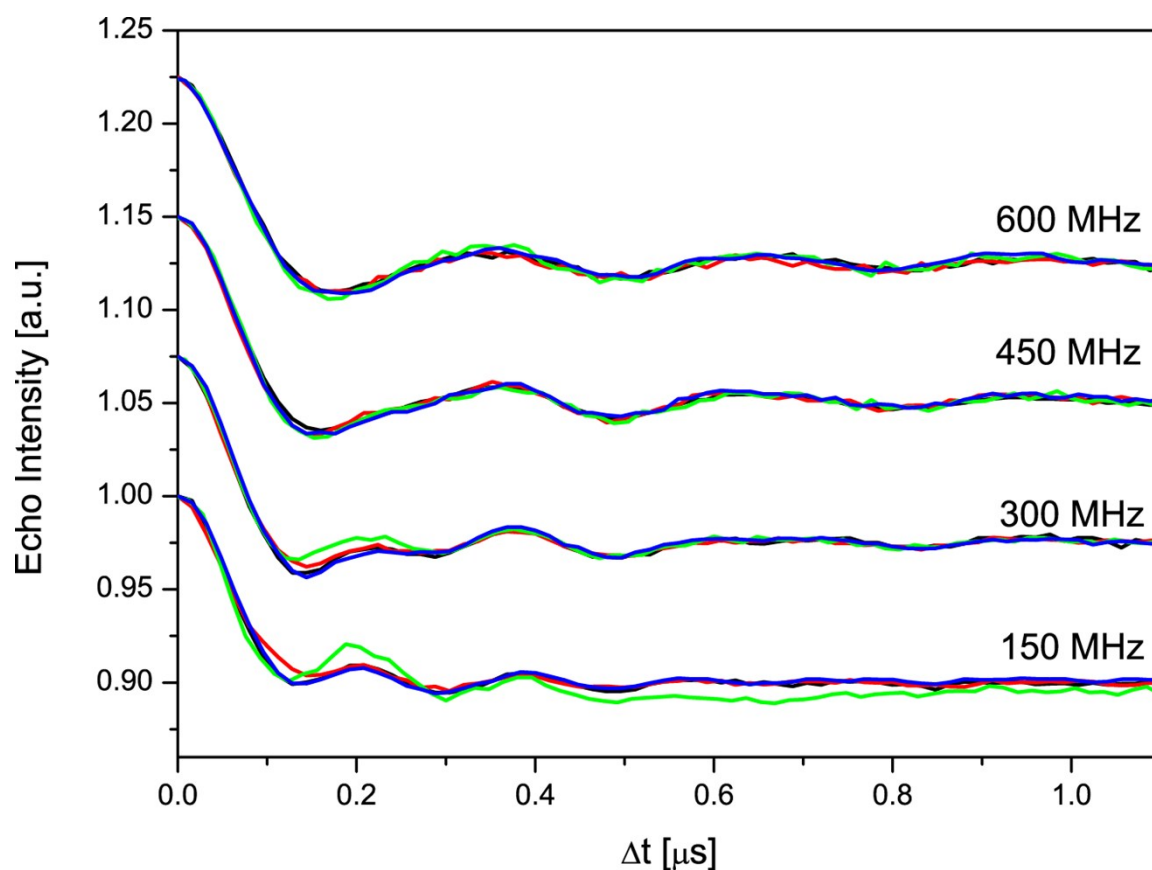


Figure S19. Background subtracted PELDOR time traces (scaled for ease of comparison to the same modulation depth of 10%) of **2x** observed on the copper center (black time trace), **2b** observed on the copper (red time trace), **2b** observed on the copper using an ELDOR attenuation of 20 dB (blue time trace) and **2b** observed on the nitroxide spin center (green time trace).

assumed. This implies that the angle between the field vector and both nitroxide copper vectors is identical. Furthermore, a distribution of distances as predicted by PeldorFit and the chemical equilibrium as described by equation (S2) was taken into account. The results of these theoretical considerations are shown in Figure S20 and Table S16.

Table S16. Observed and calculated modulation depths.

| $\Delta\nu$ [MHz] | 150 | 300 | 450 | 600 |
|-------------------------------------|-----|-----|-----|-----|
| $V\lambda_{obs}$ (2x) [%] | 40 | 31 | 24 | 21 |
| $V\lambda_{calc}$ (2x) [%] | 42 | 30 | 23 | 20 |
| $V\lambda_{obs}$ (2b) [%] | 70 | 56 | 42 | 37 |
| $V\lambda_{calc}$ (2x) [%] | 70 | 56 | 43 | 38 |

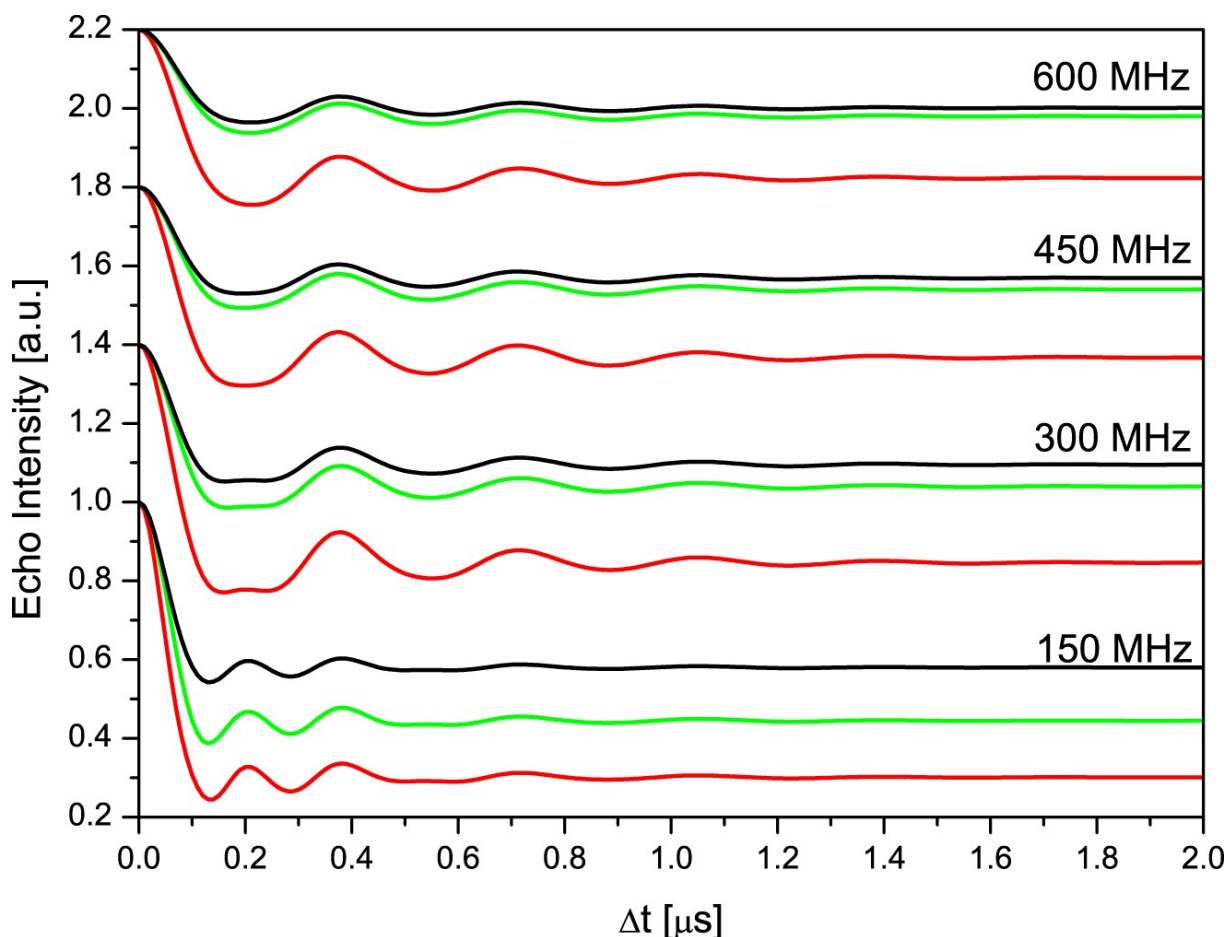


Figure S20. Calculated time traces using the orientational selectivity deduced by PeldorFit for **2x** (black lines), **2b** (red lines) and hypothetical pure two spin contribution (green lines).

Despite the simplified geometric model ($\alpha = 180^\circ$), the simulation demonstrates the absence of marked multispin effects, aside from the increase in modulation depth. If the simulated time traces shown in Figure S21 are scaled to an identical modulation depth one can observe, that the very weak deviations in the different simulated time traces occur at the same position as found experimentally, namely mostly during the first modulation period (Figure S21). Furthermore, the simulations also allow understanding the reason for the absence of marked multispin effects. The exact antiparallel orientation which was assumed in the simulations for the two nitroxide spin, leads to equal dipolar coupling frequencies for the two nitroxide-copper spin pairs in the three spin system. The combination frequencies are therefore zero and twice the expected dipolar coupling frequency for the difference and sum frequencies, respectively. Thus, the difference frequencies lead to an apparent reduction of the modulation depth, as those frequencies are subtracted with the background during data processing. The sum frequencies on the other hand could lead to deviations in the formfactor. However, the relatively low

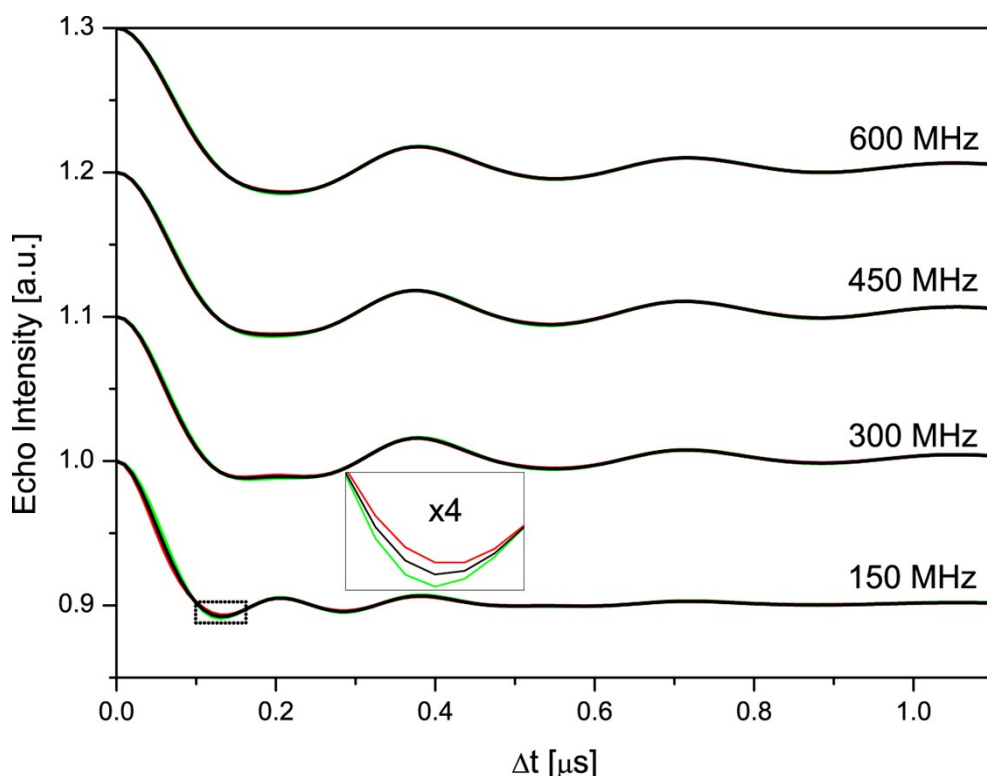


Figure S21. Calculated time traces using the orientational selectivity deduced by PeldorFit for **2x** (black lines), **2b** (red lines) and hypothetical pure two spin contribution (green lines) scaled to an identical modulation depth of 10%. The deviations are very weak and occur mostly during the first modulation period, as observed experimentally. The inset shows the marked part of the time trace in fourfold magnification.

probability for sum-frequencies which lie outside the range of frequencies which are already observed in the two-spin contribution leads to three-spin contributions which are not clearly visible in the time traces.

To conclude the discussion concerning multispin effects, the argument is summarized briefly. For different kinds of PELDOR experiments have been conducted. These experiments are measurements using the standard PELDOR set-up on **2x** (occurrence of multispin effects expected as roughly one third of the molecules are actually the threespin system **2b**), measurements using the standard PELDOR set-up on **2b** (occurrence of more pronounced multispin effects in comparison to **2x**), measurements using the standard PELDOR set-up with an ELDOR attenuation of 20 dB on **2b** (suppression of multispin effects owed to low inversion efficiency) and measurements using an inverted PELDOR set-up on **2b** (no multispin effects expected as only a single, copper centered spin is flipped by the pump pulse). None of these experiments showed marked deviations in their form factors as compared to any of the other experiments. Noteworthy, results which have

been obtained previously on a three-nitroxide spin system, in which orientation selectivity does not play a prominent role, do not show occurrence of further extrema or any shift of the position of the existing extrema in the form factor either, thereby favoring the latter explanation for the absence of marked multispin effects.^{5,6} Additionally, multispin effects have been taken into account retroactively into the PELDOR simulations, using a simple geometric model ($\alpha = 180^\circ$). The obtained theoretical time traces have modulations depths which agree with those observed experimentally. This agreement rules out a reduced probability for simultaneous spin flips, as the observed modulations depths are determined by the probability of single and simultaneous spin flips. Furthermore, the obtained theoretical time traces lack marked changes in their form factors as well. The very slight deviations occur mostly in the same regions, as those observed experimentally. Taking the results of the experiments and the theoretical considerations together strongly favors the occurrence of multispin effects which do not cause marked changes in the form factors.

References

- (1) Abdullin, D.; Hagelueken, G.; Hunter, R. I.; Smith, G. M.; Schiemann, O. *Mol. Phys.* **2014**, *113* (6), 544–560.
- (2) Meyer, A.; Schnakenburg, G.; Glaum, R.; Schiemann, O. *Inorg. Chem.* **2015**, *54* (17), 8456–8464.
- (3) Neese, F. *Wiley Interdiscip. Rev. Comput. Mol. Sci.* **2012**, *2* (1), 73–78.
- (4) Jeschke, G.; Polyhach, Y. *Phys. Chem. Chem. Phys.* **2007**, *9* (16), 1895–1910.
- (5) Von Hagens, T.; Polyhach, Y.; Sajid, M.; Godt, A.; Jeschke, G. *Phys. Chem. Chem. Phys.* **2013**, *15* (16), 5854–5866.
- (6) Giannoulis, A.; Ward, R.; Branigan, E.; Naismith, J. H.; Bode, B. E. *Mol. Phys.* **2013**, *111* (18-19), 2845–2854.